Quantum Control in the Cs $6S_{1/2}$ Ground Manifold Using Radio-Frequency and Microwave Magnetic Fields

A. Smith,[1,*] B. E. Anderson,[1] H. Sosa-Martinez,[1] C. A. Riofrío,[2,†] Ivan H. Deutsch,[2] and Poul S. Jessen[1]

[1]*Center for Quantum Information and Control, College of Optical Sciences and Department of Physics, University of Arizona, Tucson, Arizona 85721, USA*

[2]*Department of Physics and Astronomy, Center for Quantum Information and Control, University of New Mexico, Albuquerque, New Mexico 87131, USA*

(Received 20 August 2013; published 24 October 2013)

We implement arbitrary maps between pure states in the 16-dimensional Hilbert space associated with the ground electronic manifold of ^{133}Cs. This is accomplished by driving atoms with phase modulated radio-frequency and microwave fields, using modulation waveforms found via numerical optimization and designed to work robustly in the presence of imperfections. We evaluate the performance of a sample of randomly chosen state maps by randomized benchmarking, obtaining an average fidelity >99%. Our protocol advances state-of-the-art quantum control and has immediate applications in quantum metrology and tomography.

DOI: 10.1103/PhysRevLett.111.170502 PACS numbers: 03.67.−a, 02.30.Yy, 37.10.−x, 42.50.Dv

Coherent control of complex quantum systems plays a role in much of modern physics, and examples are easy to find in areas that include atomic and molecular physics [1,2], ultrafast physics [3], low temperature physics [4], and nanoscience [5,6]. In particular, high-fidelity control is a cornerstone of quantum information science, where it is an essential part of quantum-enhanced approaches to computation [7], simulation [8–10], communication [11], and metrology [12]. Because qubits are often encoded in physical spins, these tasks generally translate into control and measurement of individual and coupled spins. Atomic ground states, comprised of coupled nuclear and electronic spins, are a particularly attractive platform for quantum information science due to long coherence times and an existing, powerful toolbox for control and measurement. Examples include ion-trap quantum computers [13], neutral-atom quantum simulators [8], quantum memories [14], and spin squeezing for quantum-limited clocks and magnetometers [15].

One of the most basic tasks of quantum control is to time evolve a quantum system from a given initial to a desired final state (state mapping). In this Letter, we explore the limits of state mapping between arbitrary pure states in a large Hilbert space, using as our test bed the 16-dimensional hyperfine manifold associated with the electronic ground state of ^{133}Cs atoms. The atomic evolution is driven by static, radio-frequency (rf), and microwave (μw) magnetic fields, which is sufficient for full controllability in the entire ground manifold [16]. In contrast to past work based on the tensor light shift [17,18], this approach is not affected by decoherence due to light scattering and associated optical pumping. As a result, our state map fidelities are limited only by imperfections in the applied magnetic fields, and we show that these can be compensated with "robust" control techniques [19] analogous to those used for spin-1/2 systems in nuclear magnetic resonance [2]. Finally, we implement and test a protocol for randomized benchmarking of state maps, inspired by those developed for Clifford gates in single- and few-qubit systems [20,21]. Combining these techniques, we have implemented and benchmarked a large sample of randomly chosen state maps and measured an average fidelity of 99.11(5)%. The corresponding infidelity is smaller by a factor of 5 to 10 relative to some recent experiments with similar-sized Hilbert spaces on other platforms [22–24] and thus represents a significant advance in state-of-the-art quantum control. Such high-fidelity state mapping has important applications in quantum state preparation, e.g., known inputs for process tomography [25], states that increase the coupling strength in atom-light interfaces and improve the generation of spin squeezing [26], and custom initial states for the study of nonequilibrium dynamics in spinor quantum gases [27–29].

A detailed theoretical study of our scheme for quantum control of hyperfine-coupled electron and nuclear spins in alkali atoms can be found in Ref. [16]. The most important conclusion of that work is that controllability can be achieved with a static bias magnetic field along z, combined with phase modulated rf magnetic fields along x and y, and a phase modulated μw field driving a single transition between the hyperfine manifolds $F_\pm = I \pm 1/2$. In this context, controllability means that the Hamiltonian dynamics can generate any transformation in $SU(d)$, where $d = 2(2I + 1)$ is the Hilbert space dimension of the alkali ground manifold for nuclear spin I. In the case of ^{133}Cs, we have $I = 7/2$, and thus $F_\pm = 3, 4$ and $d = 16$. In the rotating wave approximation, taking into account the finite nuclear magnetic moment and the second order Zeeman shift from the bias field, and driving the $|F = 3, m = 3\rangle \leftrightarrow |F = 4, m = 4\rangle$ μw transition, the corresponding control Hamiltonian has the form

$$H_C = H_0 + H_{\rm rf}^{(3)}(\phi_x, \phi_y) + H_{\rm rf}^{(4)}(\phi_x, \phi_y) + H_{\mu{\rm w}}(\phi_{\mu{\rm w}}).$$

For a derivation and the full form of this Hamiltonian, see the accompanying Supplemental Material [30] and Ref. [31]. We note that H_0 is independent of the control phases ϕ_x, ϕ_y, and $\phi_{\mu\mathrm{w}}$, that $H_{\mathrm{rf}}^{(3)}$ and $H_{\mathrm{rf}}^{(4)}$ are independent $SU(2)$ rotations of the $F_\pm = 3, 4$ manifolds controlled by the phases of the rf fields, and that $H_{\mu\mathrm{w}}$ is an $SU(2)$ rotation of the $|F_\pm, m = F_\pm\rangle$ pseudospin controlled by the phase of the μw field. Using standard arguments from control theory [32,33], one can show that this is sufficient to make the system controllable. The basic idea is to start from a limited set of control Hamiltonians, generated by choosing different combinations of control phases until no additional linearly independent operators can be obtained. One then checks that these operators and their repeated commutators generate a basis for the Lie algebra $su(d)$; if so, the system is controllable. In our case, it is straightforward to do this numerically; see Ref. [16] for details.

Besides the control phases, the control Hamiltonian depends critically on an additional set of parameters $\Lambda = \{\Omega_0, \Omega_x, \Omega_y, \Omega_{\mu\mathrm{w}}, \Delta_{\mathrm{rf}}, \Delta_{\mu\mathrm{w}}\}$. Here, $\Omega_0 = 1$ MHz is the Larmor frequency at which the spin $\mathbf{F}^{(4)}$ precesses in the bias field, $\Omega_x = \Omega_y = 9$ kHz are the rf Larmor frequencies in the rotating frame, $\Omega_{\mu\mathrm{w}} = 27.5$ kHz is the microwave Rabi frequency, and $\Delta_{\mathrm{rf}} = \Delta_{\mu\mathrm{w}} = 0$ are the detunings of the rf and μw fields from resonance. As described below, our control fields are designed under the assumption that these parameters are very close to the indicated values; assuring that this is the case in the laboratory is one of the main challenges of the experiment. Details of how the parameters Λ are measured and set to their design values, as well as how their spatial and temporal inhomogeneities are estimated, can be found in Ref. [31].

Our experimental setup (Fig. 1) consists of a vapor-cell magneto-optic trap (MOT) and optical molasses, capable of preparing a few million Cs atoms at temperatures as low as 3 μK. The bias and rf magnetic fields are applied by three orthogonal coil pairs, each with a square cross section but otherwise close to the Helmholtz configuration. The dc current for the bias field is supplied by a modified, ultrastable, quasi-cw laser diode driver, while the current source for the rf fields is a dual-channel arbitrary waveform generator followed by power amplifiers. The microwave field is generated by a μw synthesizer running at 9.2 GHz, mixed with a 30 MHz signal from an arbitrary waveform generator, and amplified and radiated by two separate microwave gain horns. The use of two gain horns results in significant improvement in the homogeneity of the μw intensity across the atom cloud. Using an all-glass vacuum cell and avoiding nearby conductive and magnetizable materials allows us to modulate the 1 MHz rf fields in a bandwidth of a few hundred kHz. Finally, synchronizing the experiment at a fixed point in the 60 Hz ac power line cycle allows us to measure and compensate static and ac background magnetic fields, as described in Ref. [34]. As a result, our combined static bias and background fields along z are accurate to 20 ppm and stable to about 10 ppm (30 μG). The bias field along z makes the presence of background fields along x and y less critical, and only static compensation at the milligauss level is required here.

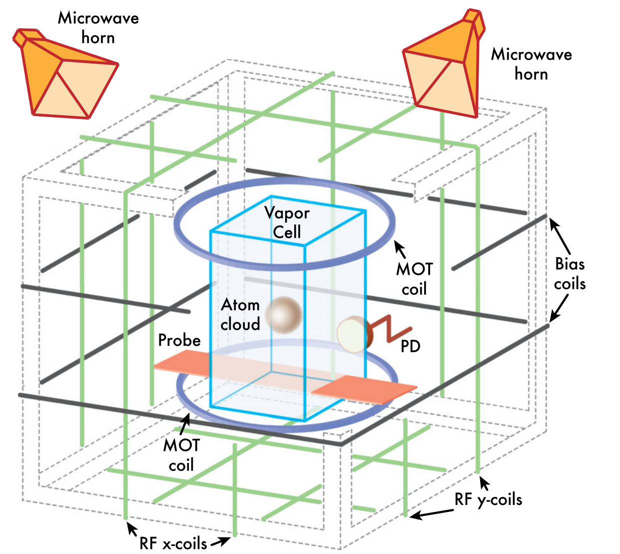

FIG. 1 (color online). Schematic of the experimental setup. Laser cooled Cs atoms are prepared in an all-glass vacuum cell centered within a plexiglas cube supporting the bias and rf coils. Microwave radiation is provided by two horn antennas. Stern-Gerlach analysis is performed by letting the atoms fall in a magnetic field gradient provided by the MOT coils and by inferring the magnetic populations from the time-dependent fluorescence excited by a probe beam and detected with a photodiode (PD).

An experimental sequence begins by releasing a cold atom sample into free fall. We use a combination of optical pumping and Larmor precession to initialize the atoms in a fiducial state $|F = 4, m = 4\rangle$, at which point the static bias field is switched on to maintain the orientation of the spin. The bias field stabilizes to the required 10 ppm level in $\sim$7 ms, at which point we apply rf and μw fields with predetermined phase modulation waveforms over a time T to evolve the spins until they closely approach the desired target state. Finally, we measure the populations in the 16 magnetic sublevels $|F, m\rangle$, by performing Stern-Gerlach analysis as described in Ref. [35] and detecting atoms in the $F_\pm$ manifolds with separate optical probe beams.

Control fields that accomplish a given state map are found using numerical techniques common to optimal control. Starting from some initial state, the goal is to find a set of time dependent phases $\{\phi_x(t), \phi_y(t), \phi_{\mu\mathrm{w}}(t)\}$ such that the fidelity relative to the target state $\mathcal{F} = |\langle\psi_{\mathrm{target}}|\psi(T)\rangle|^2$ is maximized after a fixed control time T. Maximization is done with a gradient ascent algorithm, where in each iteration the time-evolved state $|\psi(T)\rangle$ is found by numerical integration of the Schrödinger equation, starting from $|\psi_{\rm initial}\rangle$ and using the given values of the phases. To increase the speed of integration, we keep the phases piecewise constant in time, typically using 30 time steps for the μw phase and 15 time steps for each rf phase in a "control waveform" of 300 μs duration [Fig. 2(a)]. The total number of control variables (60) is thus well above the $2d-2=30$ real-valued parameters required to specify the transformation $|\psi_{\rm initial}\rangle \to |\psi_{\rm target}\rangle$. We begin the numerical search for phases $\{\phi_x^{(i)}, \phi_y^{(i)}, \phi_{\mu{\rm w}}^{(i)}\}$ with a random guess and then use a standard routine from the MATLAB optimization toolbox to iteratively maximize $\mathcal{F}$. The result is a control waveform corresponding to a local maximum in the control landscape; it is our experience that different initial guesses lead to different control waveforms, but that if T is large enough, nearly every initial guess will result in a waveform that achieves >99% fidelity. This is consistent with the expected benign nature of the search landscape [36].

The optimization procedure can be extended to find control waveforms that are robust in the presence of errors and imperfections, at the cost of a slight increase in the required control time and number of control variables. In our case, the dominant imperfections are spatial inhomogeneities and shot-to-shot variations of the parameters in H_C. A robust control waveform can then be found by maximizing the average fidelity $\bar{\mathcal{F}} = \int_\Lambda P(\Lambda)|\langle\psi_{\rm target}|\psi_\Lambda(T)\rangle|^2 d\Lambda$, where $P(\Lambda)$ is the probability that the parameters take on values Λ, and $|\psi_\Lambda(T)\rangle$ is the corresponding final state [37]. In practice, we have found it sufficient to average over three values of the bias field $\{\Omega_0, \Omega_0 \pm \delta\Omega_0\}$ and three values of the μw Rabi frequency $\{\Omega_{\mu{\rm w}}, \Omega_{\mu{\rm w}} \pm \delta\Omega_{\mu{\rm w}}\}$ for a total of nine combinations of parameter values. For simplicity, we assume each combination is equally probable and use variations $\delta\Omega_0 =$ 100 Hz and $\delta\Omega_{\mu{\rm w}} = 140$ Hz that are slightly larger than our estimated standard deviations. This relatively coarse sampling of the probability distribution speeds optimization, and we have found that the resulting, optimized control waveform performs well when its fidelity is averaged using a finer sampling of the estimated Gaussian distributions. Again, it is our experience that waveforms with fidelity in excess of 99% can almost always be found from a single initial guess. Figure 2(b) illustrates the performance of a robust control waveform designed in this fashion. The figure shows intermediate and final density matrices from a numerical simulation that includes an average over Λ, with conservative estimates for the uncertainty of every parameter. The resulting final state is very slightly mixed, but the state map fidelity remains very high.

The simplest experimental test of our state mapping protocol is to start from $|F=4, m=4\rangle$, map to any one of the states $|F, m\rangle$, and estimate the fidelity directly by measuring the population of the target state by Stern-Gerlach analysis. Figure 3(a) shows Stern-Gerlach signals for maps to each of the 16 magnetic sublevels in the ground manifold, while Figs. 3(b) and 3(c) show histograms of the estimated fidelity for 32 nonrobust and 32 robust control waveforms (the sets contain two different control waveforms for each map $|4,4\rangle \to |F,m\rangle$). The trend in these data suggests that robust waveforms slightly outperform

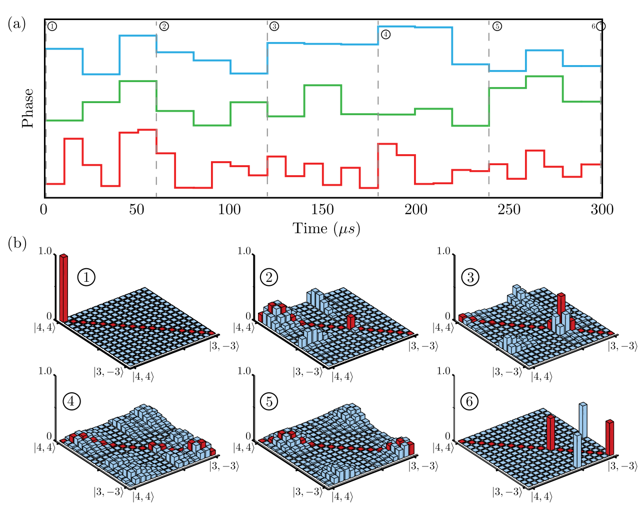

FIG. 2 (color online). Implementation of the quantum state map $|4,4\rangle \to (|3,3\rangle + |3,-3\rangle)/\sqrt{2}$. (a) Phase modulation waveform for the rf (top and middle) and μw (bottom) fields. (b) Numerical simulation of the evolving quantum state, shown as density matrices for the times indicated. Populations are shown as dark (red) tones and coherences (absolute values only) as light (blue) tones. Magnetic sublevels are ordered $\{|4,4\rangle, \ldots, |4,-4\rangle, |3,3\rangle, \ldots, |3,-3\rangle\}$ along the axes.

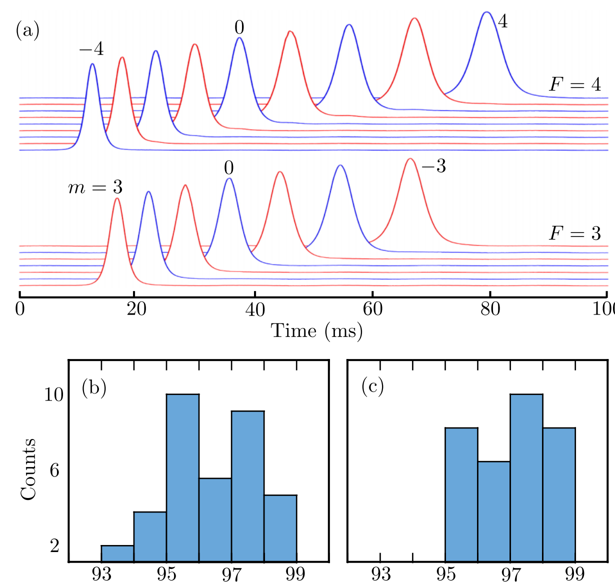

FIG. 3 (color online). (a) Stern-Gerlach analysis of magnetic sublevel populations, in the form of arrival time distributions at the probe beam. Each line is a separate measurement after a state map $|4,4\rangle \to |F,m\rangle$, as indicated. (b) Histogram of the fidelities for 32 nonrobust state maps of this form. (c) Histogram of the fidelities for 32 robust state maps of this form.

nonrobust waveforms. However, the estimated fidelities include a substantial contribution from errors in initial state preparation and final state readout, and are therefore not an accurate measure of the fidelity of the state maps themselves. Furthermore, this simple technique cannot be used to estimate the fidelity of state maps where the final state is a coherent superposition of two or more magnetic sublevels. In Ref. [38], we used the state mapping procedure discussed here to produce complex input states for tomography, and comparisons between a few (relatively low-fidelity) reconstructions and the corresponding target states can be seen there.

To obtain an accurate measure of state map fidelity, we employ a procedure inspired by the randomized benchmarking protocol developed for single- and multiqubit Clifford gates [20,21]. The basic idea is to apply state maps in progressively longer sequences, i.e.,

$$|4,4\rangle \to |\psi_0\rangle \to |4,4\rangle,$$
$$|4,4\rangle \to |\psi_0\rangle \to |\psi_1\rangle \to |4,4\rangle,$$
$$|4,4\rangle \to |\psi_0\rangle \to \cdots \to |\psi_l\rangle \to |4,4\rangle,$$

and estimate the overall fidelity of each sequence by measuring the population returned to $|4,4\rangle$. To increase sample size, we consider a number of such progressions, each consisting of different sequences with intermediate states $|\psi_0\rangle, \ldots, |\psi_l\rangle$ chosen at random according to the Haar measure [39]. For each progression, we design control waveforms to perform the corresponding state maps, implement these in the laboratory, and measure the overall fidelity as a function of l. Finally, we average together the fidelities observed for the different progressions, which improves statistics and smooths out fluctuations from accidental spin-echo effects in the individual progressions. The resulting data are fit to a function

$$\mathcal{F}(l) = \frac{1}{d} + \frac{d-1}{d}\left(1 - \frac{d}{d-1}\epsilon_0\right)\left(1 - \frac{d}{d-1}\epsilon\right)^l,$$

where $d = 16$ is the Hilbert space dimension, ϵ is the average error per state map, and ϵ_0 is the average combined error in the preparation (optical pumping into $|4,4\rangle$ and mapping $|4,4\rangle \to |\psi_0\rangle$) and readout (mapping $|\psi_l\rangle \to |4,4\rangle$ and measuring the $|4,4\rangle$ population) steps. This generalization of the fit function used for qubits [21] ensures proper asymptotic behavior for large and small l. Figure 4(a) shows typical data from this randomized benchmarking protocol, from which we infer a fidelity per state map $\mathcal{F} = 1 - \epsilon$ of 99.11(5)% and 97.7(3)% for robust and nonrobust control waveforms, respectively.

As a final step, we use numerical modeling to check that our benchmarking protocol yields average fidelities in reasonable agreement with other measures. We do this in two steps, first by generating simulated benchmarking data analogous to Fig. 4(a) and fitting them to obtain average state map errors ϵ_B, and second, by calculating

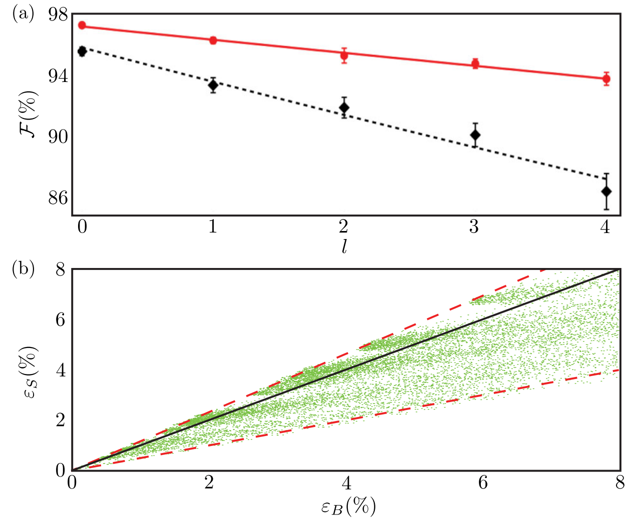

FIG. 4 (color online). (a) Randomized benchmarking data showing the overall fidelity for sequences of up to four state maps. Points are experimental data, and lines are fits of the form $\mathcal{F}(l)$, for robust (red circles) and nonrobust (black diamonds) control waveforms. Error bars are 1 standard deviation for the average over different state map sequences. The average fidelities per state map inferred from the fits are 99.11(5)% and 97.7 (3)%, respectively. (b) Plot showing the correlation between benchmarking and standard fidelities. Each data point (ϵ_B, ϵ_S) is obtained from a numerical simulation performed with a distinct set of values for the parameters in H_C. Solid and dashed lines correspond to $\epsilon_S = \epsilon_B$, $\epsilon_S = 0.5\epsilon_B$, and $\epsilon_S = 1.15\epsilon_B$, respectively.

the standard infidelities $1 - |\langle\psi_{\mathrm{target}}|\psi(T)\rangle|^2$ for the state maps used in the simulation and averaging those to obtain an average standard error ϵ_S. This process is repeated for many parameter values Λ, each time producing a data point (ϵ_B, ϵ_S) for the possible correlation between the two measures. Figure 4(b) shows a large collection of such data points for parameters Λ that go well beyond the range likely to be present in our experiment. If our benchmarking protocol is reasonable, one would expect all those data points to lie near the line $\epsilon_S = \epsilon_B$. In practice, they appear to fall mostly below that line, clustered roughly in the range $0.5\epsilon_B < \epsilon_S < 1.15\epsilon_B$. This suggests that in some situations, the benchmarking protocol may overestimate the standard error by as much as a factor of 2. In the context of our experiment, this means the average of the standard fidelity for a set of randomly chosen state maps is likely to lie between 99% and 99.5%, a result that could not have been easily established by other means.

In conclusion, we have demonstrated that high-fidelity quantum state mapping can be implemented in the 16-dimensional hyperfine ground manifold of ^{133}Cs, by driving the system solely with phase modulated rf and μw magnetic fields. Robust controls can be efficiently designed to compensate for imperfections in the driving fields, leading to significant improvements in the accuracy of the state maps. A randomized benchmarking protocol was implemented and showed that the average fidelity of such robust state maps is 99% or greater. Future use of this platform includes the exploration of control tasks that are more complex than state maps, e.g., unitary transformations on the entire ground manifold or subspaces thereof, and partial isometries that map between subspaces. Such studies will help address questions related to the feasibility of a numerical search for control waveforms that implement those types of transformations [40], as well as the possibility of inhomogeneous control and whether control can be robust in the presence of static and time-dependent perturbations [19].

This work was supported by the U.S. National Science Foundation Grants No. PHY-1212308, No. PHY-1212445, No. PHY-0903930, and No. PHY-0969997.

*Present address: HRL Laboratories LLC, 3011 Malibu Canyon Road, Malibu, CA 90265, USA.

†Present address: Dahlem Center for Complex Quantum Systems, Freie Universität Berlin, 14195 Berlin, Germany.

[1] C. Brif, R. Chakrabarti, and H. Rabitz, New J. Phys. **12**, 075008 (2010).

[2] L. M. K. Vandersypen and I. L. Chuang, Rev. Mod. Phys. **76**, 1037 (2005).

[3] F. Krausz and M. Ivanov, Rev. Mod. Phys. **81**, 163 (2009).

[4] I. Bloch, J. Dalibard, and W. Zwerger, Rev. Mod. Phys. **80**, 885 (2008).

[5] J. J. L. Morton, D. R. McCamey, M. A. Eriksson, and S. A. Lyon, Nature (London) **479**, 345 (2011).

[6] D. D. Awschalom, L. C. Bassett, A. S. Dzurak, E. L. Hu, and J. R. Petta, Science **339**, 1174 (2013).

[7] T. D. Ladd, F. Jelezko, R. Laflamme, Y. Nakamura, C. Monroe, and J. L. O'Brien, Nature (London) **464**, 45 (2010).

[8] I. Bloch, J. Dalibard, and S. Nascimbene, Nat. Phys. **8**, 267 (2012).

[9] R. Blatt and C. F. Roos, Nat. Phys. **8**, 277 (2012).

[10] A. Aspuru-Guzik and P. Walther, Nat. Phys. **8**, 285 (2012).

[11] J. O'Brien, A. Furusawa, and J. Vuckovic, Nat. Photonics **3**, 687 (2009).

[12] V. Giovannetti, S. Lloyd, and L. Maccone, Nat. Photonics **5**, 222 (2011).

[13] D. J. Wineland and D. Leibfried, Laser Phys. Lett. **8**, 175 (2011).

[14] N. Sangouard, C. Simon, H. de Riedmatten, and N. Gisin, Rev. Mod. Phys. **83**, 33 (2011).

[15] J. Ma, X. Wang, C. P. Sun, and F. Nori, Phys. Rep. **509**, 89 (2011).

[16] S. T. Merkel, P. S. Jessen, and I. H. Deutsch, Phys. Rev. A **78**, 023404 (2008).

[17] S. Chaudhury, S. Merkel, T. Herr, A. Silberfarb, I. H. Deutsch, and P. S. Jessen, Phys. Rev. Lett. **99**, 163002 (2007).

[18] I. H. Deutsch and P. S. Jessen, Opt. Commun. **283**, 681 (2010).

[19] B. E. Mischuck, S. T. Merkel, and I. H. Deutsch, Phys. Rev. A **85**, 022302 (2012).

[20] E. Knill, D. Leibfried, R. Reichle, J. Britton, R. B. Blakestad, J. D. Jost, C. Langer, R. Ozeri, S. Seidelin, and D. J. Wineland, Phys. Rev. A **77**, 012307 (2008).

[21] C. A. Ryan, M. Laforest, and R. Laflamme, New J. Phys. **11**, 013034 (2009).

[22] T. Monz, P. Schindler, J. T. Barreiro, M. Chwalla, D. Nigg, W. A. Coish, M. Harlander, W. Hänsel, M. Hennrich, and R. Blatt, Phys. Rev. Lett. **106**, 130506 (2011).

[23] K. S. Choi, A. Goban, S. B. Papp, S. J. van Enk, and H. J. Kimble, Nature (London) **468**, 412 (2010).

[24] Y. Israel, I. Afek, S. Rosen, O. Ambar, and Y. Silberberg, Phys. Rev. A **85**, 022115 (2012).

[25] I. L. Chuang and M. A. Nielsen, J. Mod. Opt. **44**, 2455 (1997).

[26] L. M. Norris, C. M. Trail, P. S. Jessen, and I. H. Deutsch, Phys. Rev. Lett. **109**, 173603 (2012).

[27] M.-S. Chang, Q. Qin, W. Zhang, L. You, and M. S. Chapman, Nat. Phys. **1**, 111 (2005).

[28] L. E. Sadler, J. M. Higbie, S. R. Leslie, M. Vengalattore, and D. M. Stamper-Kurn, Nature (London) **443**, 312 (2006).

[29] Y. Liu, S. Jung, S. E. Maxwell, L. D. Turner, E. Tiesinga, and P. D. Lett, Phys. Rev. Lett. **102**, 125301 (2009).

[30] See Supplemental Material at http://link.aps.org/supplemental/10.1103/PhysRevLett.111.170502 for a derivation and the full form of the control Hamiltonian.

[31] A. Smith, Ph.D. thesis, University of Arizona, 2012, http://arizona.openrepository.com/arizona/handle/10150/223351.

[32] V. Jurdjevic and H. J. Sussmann, J. Diff. Equ. **12**, 313 (1972).

[33] R. W. Brockett, SIAM J. Appl. Math. **25**, 213 (1973).

[34] A. Smith, B. E. Anderson, S. Chaudhury, and P. S. Jessen, J. Phys. B **44**, 205002 (2011).

[35] G. Klose, G. Smith, and P. S. Jessen, Phys. Rev. Lett. **86**, 4721 (2001).

[36] H. A. Rabitz, M. M. Hsieh, and C. M. Rosenthal, Science **303**, 1998 (2004).

[37] K. Kobzar, B. Luy, N. Khaneja, and S. J. Glaser, J. Magn. Reson. **173**, 229 (2005).

[38] A. Smith, C. A. Riofrío, B. E. Anderson, H. Sosa-Martinez, I. H. Deutsch, and P. S. Jessen, Phys. Rev. A **87**, 030102 (2013).

[39] F. Mezzadri, Not. Am. Math. Soc. **54**, 592 (2007).

[40] K. W. Moore, R. Chakrabarti, G. Riviello, and H. Rabitz, Phys. Rev. A **83**, 012326 (2011).